How to cite: *Angew. Chem. Int. Ed.* **2021**, *60*, 16178–16183
International Edition: doi.org/10.1002/anie.202104924
German Edition: doi.org/10.1002/ange.202104924

Molecular Recognition **Hot Paper**

A Synthetic Galectin Mimic

*Brian J. J. Timmer, Arjaan Kooijman, Xander Schaapkens, and Tiddo J. Mooibroek**

Abstract: *Galectins are a galactoside specific subclass of carbohydrate binding proteins (lectins) involved in various cellular activities, certain cancers, infections, inflammations, and many other biological processes. The molecular basis for the selectivity of galectins is well-documented and revolves around appropriate interaction complementarity: an aromatic residue for C–H···π interactions and polar residues for (charge assisted) hydrogen bonds with the axial hydroxyl group of a galactoside. However, no synthetic mimics are currently available. We now report on the design and synthesis of the first galectin mimic (**6**), and show that it has a higher than 65-fold preference for n-octyl-β-galactoside (**8**) over n-octyl-β-glucoside (**7**) in CD_2Cl_2 containing 5% $[D_6]$DMSO (with $K_a \geq 4500\ M^{-1}$ for **6**:**8**). Molecular modeling informed by nOe studies reveal a high degree of interaction complementarity between **6** and galactoside **8**, which is very similar to the interaction complementarity found in natural galectins.*

Introduction

Galectins are a galactoside-selective subclass of lectins (carbohydrate binding proteins)[1] and play an important role: in regulating cellular activities;[2] in certain cancers,[3] infections,[4] and inflammations;[5] and in heart (dis)functioning[6] and liver fibrosis.[7] Technologies to study, monitor or intervene in such processes are predicated on our ability to selectively bind galactosides. The affinities of galectins towards simple saccharides is typically in the order of $K_a \approx 10^3\ M^{-1}$ for disaccharides,[8] even less for galactose itself, while immeasurably small for a carbohydrate such as glucose.[8c] The structural characteristics that underpin the selectivity of galectins for galactosides are well-understood and involve a well-preserved[1b,9] tryptophan residue for C–H···π interactions,[10] together with several polar residues for hydrogen bonding (HB) with hydroxyl groups. This is illustrated in Figure 1a for human galectin-3[1d,5b,6–7,9] in complex with *N*-acetyl-D-lactosamine (PDB-code 1A3K).[9] In Figure 1a, the C–H···π interactions with tryptophan-181 are shown in magenta and the HB interaction between asparagine-174 and the galactoside methylene OH are shown in green. The selectivity for galactosides stems largely from the HBs between histidine-158/arginine-162 and the axial hydroxyl at the 4-postion (in blue). This axial hydroxyl is equatorially oriented in analogous O-linked β-glucosides (Figure 1b), thus rationalising the selectivity.

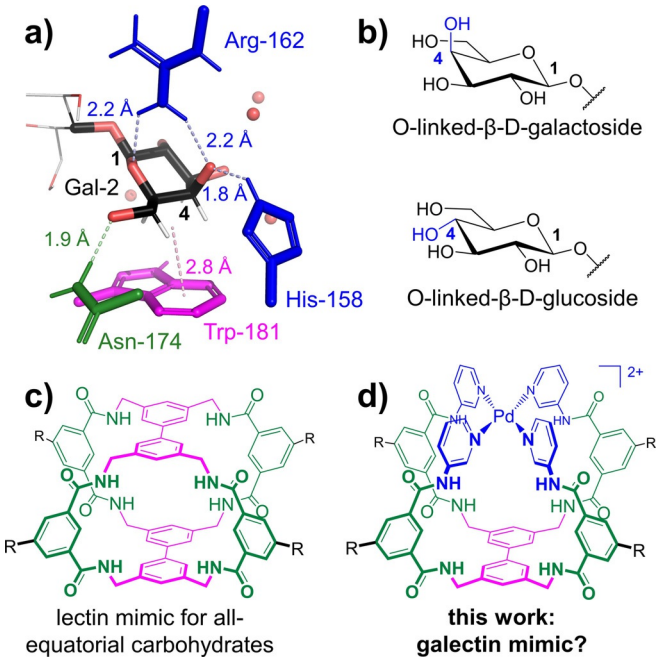

Figure 1. a) Galactoside binding domain of human galectin-3 (1A3K) bound to the galactose residue of *N*-acetyl-D-lactosamine (H-bonded water molecules are shown as red spheres). b) The structures of O-linked β-D-glucoside/galactoside with OH-4 highlighted in blue. c) Covalent cage as lectin mimic for all-equatorial carbohydrates. d) New design presented here aimed to mimic galectins. R = solubility handle.

Despite the well-known origin for their selectivity, there are no galectin mimics reported to date.[11] There does exist an interesting class of lectin-mimics that target the all-equatorial family of carbohydrates.[12] One such "temple" design is illustrated in Figure 1c.[12a,c,e] In this particular covalent macrocycle, two aromatic biphenyl surfaces (magenta) are separated by polar isophthalamide units (green). Despite their successes,[12f,g,i,l,n] the synthetic routes towards these macrocycles require at least one macrocyclization reaction near the end of the synthesis Scheme, which rarely surpassed 20% yield. Moreover, it is not obvious how the selectivity of this design can be fine-tuned to accommodate axial hydroxyl substituents. To remedy these drawbacks and inspired by recent reports about the carbohydrate binding properties of M_2L_4 coordination cages,[13] we designed the system shown in Figure 1d. It was envisioned that synthesis of the parent

[*] Dr. B. J. J. Timmer, A. Kooijman, X. Schaapkens, Dr. T. J. Mooibroek
Van't Hoff Institute for Molecular Sciences, University of Amsterdam
Science Park 904, 1098 XH, Amsterdam (The Netherlands)
E-mail: t.j.mooibroek@uva.nl
Supporting information and the ORCID identification number(s) for the author(s) of this article can be found under: https://doi.org/10.1002/anie.202104924.

tetradentate ligand would give a quantitative cyclization product upon reaction with a square-planar metal such as Pd^{II}. Moreover, the design was anticipated to compliment the structure of certain carbohydrates, such as galactosides, by providing an aromatic biphenyl surface (magenta), polar isophthalamide spacers (green) and a cationic $[Pd(pyridyl)_4]^{2+}$ complex for charge assisted CH hydrogen bonding to an axial hydroxyl group.[13c,14]

Results and Discussion

As is shown in Scheme 1, the synthesis of **5** was realized by reaction of pentafluorophenyl(PFP)-activated isophthalamide derivative **1** with tetra amine salt **2**,[15] followed by a derivatization of the resulting PFP-ester **3** using 3-aminopyridine **4**. After the reaction forming **3**, most of the unreacted starting material **1** could be recovered during column chromatographic purification of **3**. Tetrapyridyl ligand **5** could also be isolated with conventional silica gel column chromatography.

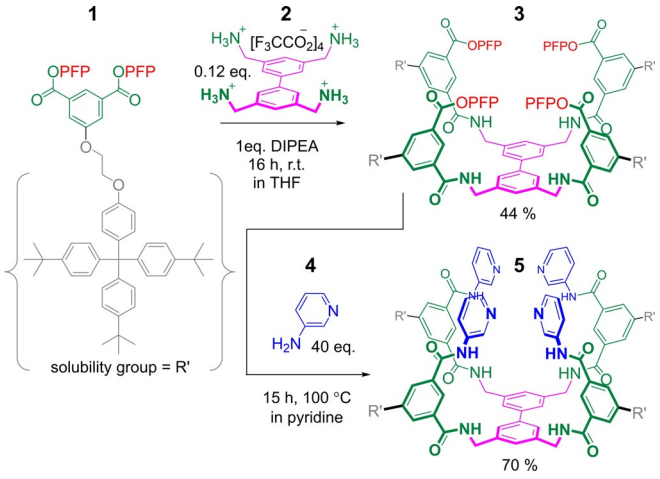

Scheme 1. Synthesis of tetrapyridyl ligand **5**. PFP = pentafluorophenyl, DIPEA = *N*,*N*-diisopropylethylamine, THF = tetrahydrofuran. The given yields in percentages (bottom) are non-optimized isolated yields. Compound **1** can be prepared on multiple gram scale in > 30% isolated yield from *p*-bromo-*t*-butylbenzene as detailed in the Supporting Information.

The identity of **5** was verified by various NMR techniques (Supporting Information, Section S2d) and high resolution mass spectroscopy. Stepwise addition of 1 equivalent a Pd^{2+} source to **5** (Figure 2a), resulted in the signal of **5** disappearing and a new set of resonances appearing. These resonances are consistent with formation of the cage-like complex **6** illustrated Figure 2b. For example, the large shifts for **s3-NH** (10.04 → 10.55 p.p.m.) **p2** (8.74 → 9.75 p.p.m.) and **p3**/**p5** (ca. 8.17 → 8.89 and 8.28 p.p.m.) are congruent with Pd-coordination of the aminopyridyl moieties of **5**.[13c,d] What also stands out from these spectra is that the singlet of the α-methylene proton **b3α** (4.46 p.p.m.) is desymmetrized to two multiplets around 4.68 and 4.51 p.p.m.. This is typical for cage-formation, which renders the methylene hydrogens diastereotopic.[12g,i] Analysis of the 2D-NOESY NMR spectrum of the newly formed species was also fully consistent with the structure of **6** (Figure S31). In particular, as is illustrated in Figure 2c, one half of the desymmetrized **b3α** had a nuclear Overhauser effect (nOe) cross peak with **b4**; not with **b2**. This [**b3α**; **b4**] nOe involves four **b3α** hydrogens that can be seen as pointing "inwards" with respect to the portal formed by **b4**, **s4** and **p2**. The other half of the desymmetrized **b3α** must be facing "outwards" relative to the **b4**/**s4**/**p2** portal and indeed has an nOe with **b2**, not **b4**. Moreover, DOSY-NMR of **6** and **5** (Figure S30) shows that both have a very similar diffusion constant, thus excluding larger structures with multiple Pd^{2+} nuclei.

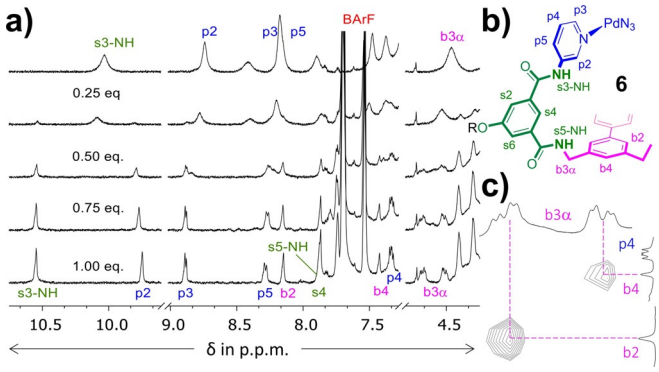

Figure 2. a) Formation of **6** (bottom) from **5** (top) by addition of the indicated equivalent of $Pd(BArF)_2$, as followed by ^1H NMR (spectra partially assigned). Solvent is 5% $[D_6]DMSO$ in CD_2Cl_2. b) Representation and labeling of **6**; c) partial NOESY spectrum of **6** zoomed-in on the nOe's between **b3α** and **b2**/**b4**. See the Supporting Information, Figures S28–S33 for complete spectra and full assignments.

As is detailed in Section S5a of the Supporting Information, a molecular model of **6** was based on the observed NOESY spectrum and calculated using density functional theory (DFT). Two space-filling representations of this model are shown in Figure 3, as viewed along the smaller portal involving **b4** (Figure 3a) and the larger portal involving **b2** (Figure 3b). As intended, the interior of **6** provides a flat aromatic biphenyl surface at the "bottom" (Figure 3c, magenta) and an uneven surface formed by the cationic $[Pd(pyridyl)_4]^{2+}$ at the "top" (Figure 3d, blue). Both are held together by the four polar isophthalamides (green). The inner dimensions of this model for **6** are generally congruent with the size of a carbohydrate (Figure S51). In particular, the internal height of **6** of 4.0–5.4 Å is in between the typical height of amide-linked covalent carbohydrate receptors (3.9 Å) and a related urea-linked glucose receptor (5.5 Å).[12l]

The ^1H NMR spectra of $[\mathbf{6}][BArF]_2$ between 0.8 and 3.0 mM (Figure S36) showed minute shifts ($\Delta\delta^{max} = 0.05$ p.p.m.) of the resonances in the aromatic region. The most significant shift was observed for **s5-NH**, yet all shifts were linear when plotted as a function of concentration (Figure S37). It was thus assumed that any self-association is negligible in this concentration range. In a control titration experiment with phenol (see also entry 1 in Table 1), similar small shifts were observed that were ascribed to the varying concentration during the experiment.

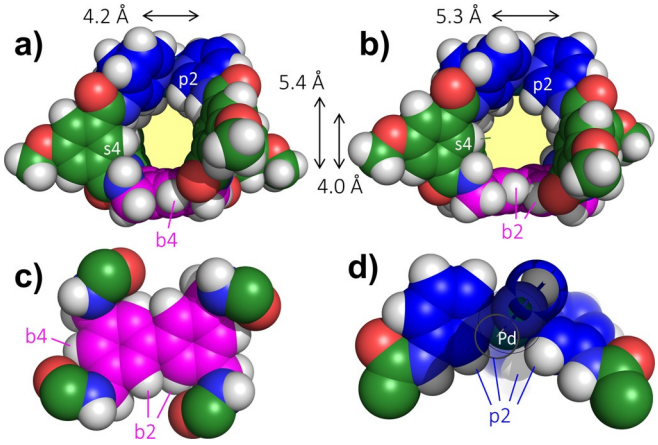

Figure 3. Molecular model of **6** with partial assignment as calculated with DFT (ωB97X-D/ 6-31G*) and viewed: a) facing the smaller **p2**/**s4**/**b4** portal; b) facing the larger **p2**/**s2**/**b2** portal; c) from the interior looking down at the flat biphenyl; d) from the interior looking at the uneven surface of the $[Pd(pyridyl)_4]^{2+}$ complex. The solubilizing groups are omitted and the distances are corrected for the van der Waals radii of the atoms. See also the Supporting Information, Section S5a for details.

Table 1: Overview of binding studies performed between [**6**][BArF]$_2$ and phenol and *n*-octyl-glycosides **7**–**10** with axial groups highlighted in blue.

Guest	5% [D$_6$]DMSO in CD_2Cl_2 Entry	K_a [M^{-1}]	10% [D$_6$]DMSO in CD_2Cl_2 Entry	K_a [M^{-1}]
phenol	1	–[a]	6	–[a]
7	2	67[b]	7	–[a]
8	3	≥4500 ± 23%[c]	8	550 ± 5%[b,c]
9	4	21[b]	9	–[a]
10	5	16[b]	10	–[a]

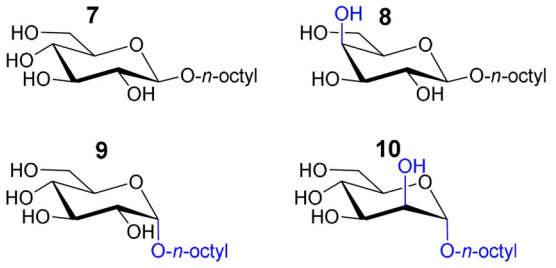

[a] Insignificant peak shifts similar to dilution were observed and the data could not be fitted to a 1:1 binding constant. At best, we estimate such constants to be in the order of < 5M-1. [b] $r^2 \geq 0.97$. [c] Determined by integration as detailed in the Supporting Information. The larger error of 23% is probably due to integration issues. See the Supporting Information, Section S3 for all titrations.

The titration with *n*-octyl-β-D-glucoside **7** in 5% [D$_6$]DMSO in CD_2Cl_2 (entry 2 in Table 1) appeared markedly different compared to addition of phenol and selected ^{1}H NMR spectra of the titration are shown in Figure 4a.

With increasing concentration of **7**, most resonances of **6** shifted. For example, the inwards facing **s3-NH**, **p2**, **s4 and s5-NH** shifted significantly and broadened somewhat near the end of the titration. The doublet of **p3** (ca. 8.89 p.p.m.) and the singlet of **b2** (ca. 8.15 p.p.m.) appear to fully split into, respectively, two doublets and two singlets. Such splitting is in line with a symmetrical molecule such as **6** hosting an asymmetrical guest like **7** in fast exchange.[12g] The methylene resonances of **b3α** also shifted and broadened. As is shown in the inset Figure of Figure 4a, these data could be fitted to a 1:1 binding model with a K_a of 67 M^{-1}. Interestingly, addition of approximately one equivalent of galactoside **8** to **6** resulted in the disappearance of most signals (Figure 4b). All resonances reappear -albeit broadened- upon cooling the sample to −30 °C (top spectrum in Figure 4b) and disappear again when heated to room temperature (see Figure S40). Integration of the disappearing resonances of **s3-NH** (ca. 10.54 p.p.m.) and **p2** (ca. 9.75 p.p.m.) plotted against the concentration of **8** could be fitted to a 1:1 model suggesting $K_a \approx 4500$ M^{-1}, but with an excessive error of 23%. This large error likely originates from integration difficulties (see Figure S40 for details), but the order of magnitude is clearly around $\geq 10^3$–10^4 M^{-1} and **6** thus appears to be selective for

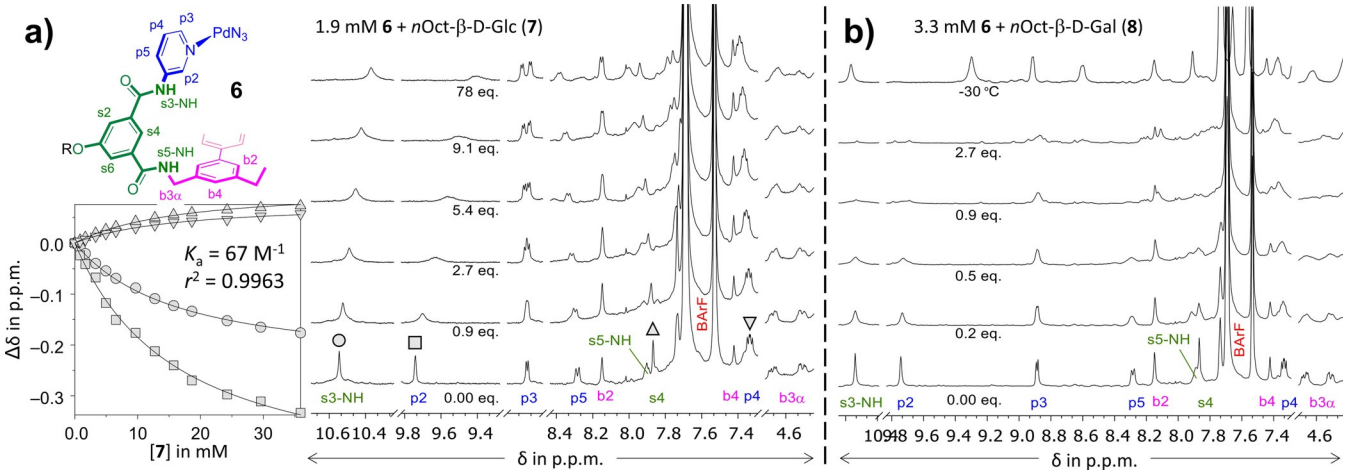

Figure 4. a) Partial ^{1}H NMR spectra and HypNMR curve fitting analysis of 1.9 mM [**6**][BArF]$_2$ titrated with glucoside **7**. Fitting was done on protons **s3-NH**, **p3**, **s4**, and **p4**, giving $K_a = 67$ M^{-1} with $r^2 = 0.9963$ over all 52 data points. b) Partial ^{1}H NMR spectra of 3.3 mM [**6**][BArF]$_2$ titrated with galactoside **7** up to about three equivalents. The top spectrum is taken at the end of the titration at −30 °C. The solvent is in CD_2Cl_2 with 5% [D$_6$]DMSO. See also the Supporting Information, Figure S39 and Figure S40.

galactoside **8** over glucoside **7** in this medium. The binding studies with the α-O-linked *n*-octyl glycosides **9** (Figure S41) and **10** (Figure S42) also displayed concentration dependent spectral changes such as shifting and broadening of resonances. The observed shifts could be fitted to a 1:1 binding model with $K_a = 21\ M^{-1}$ for **9** and $16\ M^{-1}$ for **10** (see also entries 4,5 in Table 1). These data suggest that **6** is more selective for β-O-linked *n*-octyl glycosides **7** and **8** than α-*n*-octyl glycosides **9** and **10**. Moreover, the cage is not merely selective for carbohydrates with an axial hydroxyl but very specific for galactoside **8** (compare with mannoside **10**).

As the affinity of **6** towards galactoside **8** appeared so much higher than the others, yet could not be accurately quantified in the solvent mixture used, the titrations were repeated in 10% [D_6]DMSO in CD_2Cl_2 and the results are summarized in entries 6–10 of Table 1. In the case of phenol (Figure S43) only marginal shifts were observed, in line with the lack of binding already observed in 5% [D_6]DMSO in CD_2Cl_2 (Table 1, entry 1).

For the carbohydrates **7** (Figure S45), **9** (Figure S47) and **10** (Figure S48) the shifts were somewhat larger than for phenol, yet far less than observed with these carbohydrates in 5% [D_6]DMSO in CD_2Cl_2. In particular, peak broadening was hardly observed and the splitting of resonances observed for glucoside **7** was far less than observed in 5% [D_6]DMSO in CD_2Cl_2. These data are consistent with very weak binding of **7**, **9** and **10** in the regime preceding appreciable saturation. Interestingly, in the titration with galactoside **8** (Figure S46), most of the resonances of **6** again disappeared. In this matrix, the data could be fitted accurately (±5% based on integration) to a 1:1 binding constant of about $550\ M^{-1}$, confirming the selectivity of **6** towards galactoside **8**.

To verify if the observed spectral changes were indeed caused by binding of glycosides, a series of selective 1D nOe spectra were measured in 5% [D_6]DMSO in CD_2Cl_2 of the final titration solutions in the titration with glucoside **7** at room temperature and galactoside **8** at −30 °C. As can be seen in the resulting spectra in Figure 5, excitation of the outwards facing **p3** did not result in significant nOe spin transfer with resonances in the pyranose region around 4 p.p.m. (highlighted in green). In sharp contrast, irradiation of **b2** and the inwards facing **s4** gave clear nOe's with the pyranose regions of both **7** and **8**. These nOe data thus provide evidence that binding with **7** and **8** is genuine and in particular the nOe with **s4** evidences binding to the interior of **6**.

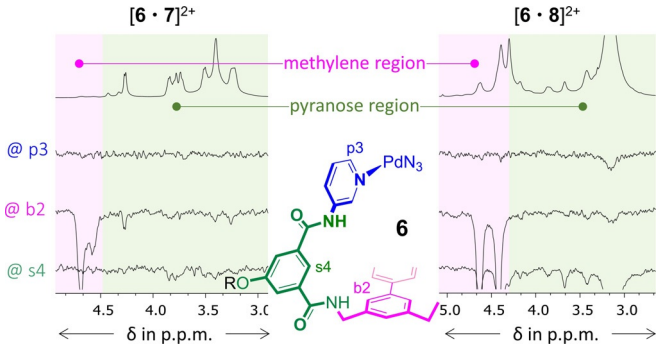

Figure 5. Partial ^{1}H NMR spectrum of [**4**·**7**][BArF]$_2$ at 25 °C and [**4**·**8**]-[BArF]$_2$ at −30 °C together with selective 1D nOe's recorded at the same temperature after excitation of **p3**, **b2** or **s4** (t_m = 350 ms). The large signal at 3.16 p.p.m. in the sample with **8** at −30 °C is from water.

As is detailed in Section S5b, molecular modeling consistent with the nOe data was used to obtain likely approximate geometries of **6** bound to glycosides **7** and **8**. Perspective views of these models are shown in Figure 6. As is highlighted in the right-hand side of Figure 6a for [**6**·**7**]$^{2+}$, bifurcated HB interactions[16] are a common structural feature. This is structurally similar to bifurcated HBs between ureas and carbohydrates.[11b,13d] The highlighted example involves a pyridyl CH (**p2**) of ring A and the NH of the connected amide (**s3-NH**), both bound to the O-atom of methylene OH-6. This same pattern is observed with ring B and O-5 of the pyranose ring, yet no HB was present at all with rings C and D in the [**6**·**7**]$^{2+}$ model. In [**6**·**8**]$^{2+}$ (Figure 6b, right), bifurcated HBs are present with rings A and C, and ring D is only involved in a HB between the amide NH and O-5. Ring B is involved in a CH···O and NH···O HB with O-1 and O-5 respectively (not shown). Hydrogen bonding interactions involving the amides connected to the biphenyl ring are less numerous and not shown in the Figure (see Figure S53 for full details). Besides hydrogen bonding, both models display CH-π interactions between the CH-moieties of the pyranose rings and the biphenyl (magenta).

As can be seen in Figure 6b, accommodating the flat CH-surface of galactoside **8** leaves the hydroxyls OH-4 and OH-2 oriented towards the coarse CH/NH surface provided by the [Pd(pyridyl)$_4$]$^{2+}$ moiety in **6** (see also Figure 3). A similar complementarity is present for O1 and O5 (not shown here,

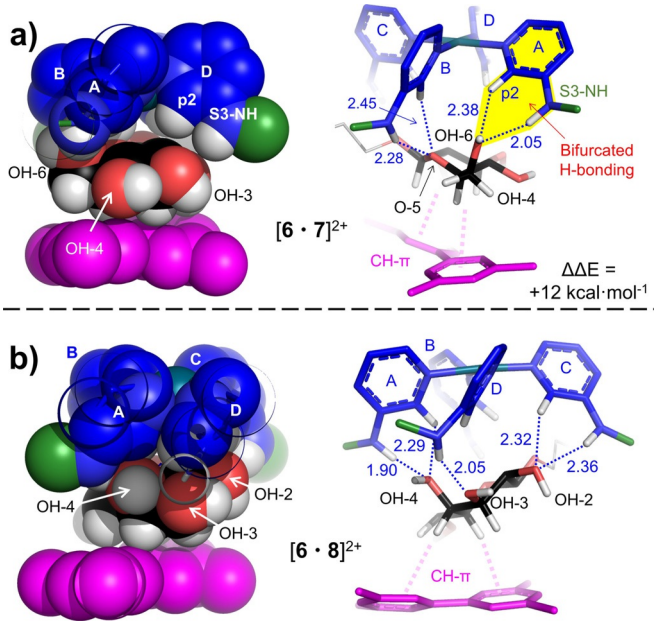

Figure 6. a) Truncated view of a molecular model of [**6**·**7**]$^{2+}$ in space-filling mode (left) and as capped sticks visualizing four of the seven HB interactions found. b) idem for [**6**·**8**]$^{2+}$ with five out of ten HBs. Both models were DFT optimized (ωB97X-D/ 6-31G*) and the complex with **7** was calculated to be 12 kcal mol^{-1} less stable. Only polar hydrogens and hydrogens involved in CH–π interactions are shown for simplicity. See the Supporting Information, Section S5b for full details.

see Figure S53b for details). By accommodating the flat CH-surface of glucoside **7** on the other hand, all hydroxyls directly connected to the pyranose ring are equatorially oriented and are thus unable to connect to the CH/NH surface of the $[Pd(pyridyl)_4]^{2+}$ moiety. This is different for the methylene hydroxyl OH-6 of **7**, which actually adopts a pseudo-axial orientation to establish the bifurcated HB highlighted in Figure 6a. It is noteworthy that $[\mathbf{6}\cdot\mathbf{8}]^{2+}$ was computed to be about 12 kcal mol^{-1} more stable than $[\mathbf{6}\cdot\mathbf{7}]^{2+}$ and has ten instead of seven HBs (see also Figure S53). While this relative energy is likely inflated due to the computational method, these models do provide a rationale for the observed selectivity of **6** for **8** in terms of relative stability and increased interaction complementarity (see also Figure S54a). Moreover, the orientation of **8** is nearly identical to that found in galectins[1b,9] such as 1A3K highlighted in Figure 1a (see also Figure S54b for a partial structure overlay).

Conclusion

In summary, a Nature-inspired synthetic galectin mimic (**6**) was designed, synthesized and shown to bind selectively to galactoside **8** in CD_2Cl_2 containing 5% or 10% $[D_6]$DMSO ($^v/_v$). The selectivity of **6** for **8** versus glucoside **7** is at least 65 (ca. 4500/67) and even larger versus α-glycosides **9** and **10** (up to 280 ca. 4500/16). A selectivity exceeding 1:65 is rare for galectins[8] and also remarkable when compared to covalent macrocycles targeting all-equatorial carbohydrates; these rarely exceed[12l] a 20-fold selectivity *against* galactose.[11b] The selectivity of **6** for **8** can be rationalized by the modeled interaction complementarity, revealing CH···π interactions and ample (charge assisted) hydrogen bonding interactions that are much like those observed in natural lectins. It must be noted that the synthesis route to **6** can easily be diverted to a diverse range of variants. For example, the solubility handle could be tweaked to make the binding core of **6** water-soluble, or the pyridyl rings can be replaced by (2-)substituted pyridyls for altered properties of the $[Pd(pyridyl)_4]^{2+}$ moiety. Another prospect is the replacement of the square-planar Pd^{II} by octahedral metals that might aid in binding via an axial vacant site.

It is concluded that **6** represents the first synthetic galectin mimic and provides a platform that opens the venue towards the preparation of a new family of carbohydrate binding molecules that can target carbohydrates with axial substituents (such as galactosides).

Notes: In addition to the nOe data, the spectra of **6** containing about 1 mM of a carbohydrate revealed significantly broadened peaks of **7**–**10** compared to spectra of pure carbohydrates at the same concentration. This too is highly indicative of binding (see Figure S49).

Acknowledgements

This research was financially supported by the Netherlands Organization for Scientific Research (NWO) with VIDI grant number 723.015.006.

Conflict of interest

The authors declare no conflict of interest.

Keywords: carbohydrate recognition · carbohydrates · galactosides · galectin mimic · molecular recognition

[1] a) S. H. Barondes, V. Castronovo, D. N. W. Cooper, et al., *Cell* **1994**, *76*, 597–598; b) S. H. Barondes, D. N. W. Cooper, M. A. Gitt, et al., *J. Biol. Chem.* **1994**, *269*, 20807–20810; c) H. Leffler, S. Carlsson, M. Hedlund, et al., *Glycoconjugate J.* **2002**, *19*, 433–440; d) J. Dumic, S. Dabelic, M. Flogel, *Biochim. Biophys. Acta Gen. Subj.* **2006**, *1760*, 616–635; e) L. Johannes, R. Jacob, H. Leffler, *J. Cell Sci.* **2018**, *131*, 9.

[2] a) N. L. Perillo, K. E. Pace, J. J. Seilhamer, et al., *Nature* **1995**, *378*, 736–739; b) N. L. Perillo, M. E. Marcus, L. G. Baum, *J. Mol. Med.* **1998**, *76*, 402–412; c) R. C. Hughes, *Biochimie* **2001**, *83*, 667–676; d) F. T. Liu, R. J. Patterson, J. L. Wang, *Biochim. Biophys. Acta Gen. Subj.* **2002**, *1572*, 263–273.

[3] a) A. Danguy, I. Camby, R. Kiss, *Biochim. Biophys. Acta Gen. Subj.* **2002**, *1572*, 285–293; b) F. T. Liu, G. A. Rabinovich, *Nat. Rev. Cancer* **2005**, *5*, 29–41; c) F. C. Chou, H. Y. Chen, C. C. Kuo, et al., *Int. J. Mol. Sci.* **2018**, *19*, 11.

[4] a) G. R. Vasta, *Nat. Rev. Microbiol.* **2009**, *7*, 424–438; b) T. L. M. Thurston, M. P. Wandel, N. von Muhlinen, et al., *Nature* **2012**, *482*, 414-U1515.

[5] a) G. A. Rabinovich, L. G. Baum, N. Tinari, et al., *Trends Immunol.* **2002**, *23*, 313–320; b) N. C. Henderson, T. Sethi, *Immunol. Rev.* **2009**, *230*, 160–171; c) F. T. Liu, G. A. Rabinovich in *Year in Immunology 2*, *Vol. 1183* (Ed.: N. R. Rose), Wiley-Blackwell, Malden, **2010**, pp. 158–182.

[6] a) U. C. Sharma, S. Pokharel, T. J. van Brakel, et al., *Circulation* **2004**, *110*, 3121–3128; b) J. E. Ho, C. Y. Liu, A. Lyass, et al., *J. Am. Coll. Cardiol.* **2012**, *60*, 1249–1256.

[7] N. C. Henderson, A. C. Mackinnon, S. L. Farnworth, et al., *Proc. Natl. Acad. Sci. USA* **2006**, *103*, 5060–5065.

[8] a) H. Leffler, S. H. Barondes, *J. Biol. Chem.* **1986**, *261*, 119–126; b) J. T. Powell, *Biochem. J.* **1980**, *187*, 123–129; c) R. F. Cerra, M. A. Gitt, S. H. Barondes, *J. Biol. Chem.* **1985**, *260*, 10474–10477.

[9] J. Seetharaman, A. Kanigsberg, R. Slaaby, et al., *J. Biol. Chem.* **1998**, *273*, 13047–13052.

[10] a) W. I. Weis, K. Drickamer, *Annu. Rev. Biochem.* **1996**, *65*, 441–473; b) M. Brandl, M. S. Weiss, A. Jabs, et al., *J. Mol. Biol.* **2001**, *307*, 357–377; c) Z. R. Laughrey, S. E. Kiehna, A. J. Riemen, et al., *J. Am. Chem. Soc.* **2008**, *130*, 14625–14633; d) L. M. Salonen, M. Ellermann, F. Diederich, *Angew. Chem. Int. Ed.* **2011**, *50*, 4808–4842; *Angew. Chem.* **2011**, *123*, 4908–4944; e) J. L. Asensio, A. Arda, F. J. Canada, et al., *Acc. Chem. Res.* **2013**, *46*, 946–954; f) W. T. Chen, S. Enck, J. L. Price, et al., *J. Am. Chem. Soc.* **2013**, *135*, 9877–9884; g) K. L. Hudson, G. J. Bartlett, R. C. Diehl, et al., *J. Am. Chem. Soc.* **2015**, *137*, 15152–15160.

[11] a) R. P. Bonar-Law, A. P. Davis, B. A. Murray, *Angew. Chem. Int. Ed. Engl.* **1990**, *29*, 1407–1408; *Angew. Chem.* **1990**, *102*, 1497–1499; b) A. P. Davis, *Chem. Soc. Rev.* **2020**, *49*, 2531–2545; c) O. Francesconi, S. Roelens, *ChemBioChem* **2019**, *20*, 1329–1346.

[12] a) A. P. Davis, R. S. Wareham, *Angew. Chem. Int. Ed.* **1998**, *37*, 2270–2273; *Angew. Chem.* **1998**, *110*, 2397–2401; b) A. P. Davis, R. S. Wareham, *Angew. Chem. Int. Ed.* **1999**, *38*, 2978–2996; *Angew. Chem.* **1999**, *111*, 3160–3179; c) E. Klein, M. P. Crump, A. P. Davis, *Angew. Chem. Int. Ed.* **2005**, *44*, 298–302; *Angew. Chem.* **2005**, *117*, 302–306; d) Y. Ferrand, M. P. Crump, A. P. Davis, *Science* **2007**, *318*, 619–622; e) Y. Ferrand, E. Klein, N. P. Barwell, et al., *Angew. Chem. Int. Ed.* **2009**, *48*, 1775–1779; *Angew. Chem.* **2009**, *121*, 1807–1811; f) C. F. Ke, H. Destecroix,

M. P. Crump, et al., *Nat. Chem.* **2012**, *4*, 718 – 723; g) T. J. Mooibroek, J. M. Casas-Solvas, R. L. Harniman, et al., *Nat. Chem.* **2016**, *8*, 69 – 74; h) T. J. Mooibroek, M. P. Crump, A. P. Davis, *Org. Biomol. Chem.* **2016**, *14*, 1930 – 1933; i) P. Rios, T. S. Carter, T. J. Mooibroek, et al., *Angew. Chem. Int. Ed.* **2016**, *55*, 3387 – 3392; *Angew. Chem.* **2016**, *128*, 3448 – 3453; j) P. Ríos, T. J. Mooibroek, T. S. Carter, et al., *Chem. Sci.* **2017**, *8*, 4056 – 4061; k) P. Stewart, C. M. Renney, T. J. Mooibroek, et al., *Chem. Commun.* **2018**, *54*, 8649 – 8652; l) R. A. Tromans, T. S. Carter, L. Chabanne, et al., *Nat. Chem.* **2019**, *11*, 52 – 56; m) O. Francesconi, F. Cicero, C. Nativi, et al., *ChemPhysChem* **2020**, *21*, 257 – 262; n) O. Francesconi, M. Martinucci, L. Badii, et al., *Chem. Eur. J.* **2018**, *24*, 6828 – 6836; o) O. Francesconi, M. Gentili, C. Nativi, et al., *Chem. Eur. J.* **2014**, *20*, 6081 – 6091; p) C. Nativi, O. Francesconi, G. Gabrielli, et al., *Chem. Eur. J.* **2012**, *18*, 5064 – 5072.

[13] a) M. Han, D. M. Engelhard, G. H. Clever, *Chem. Soc. Rev.* **2014**, *43*, 1848 – 1860; b) M. Yamashina, M. Akita, T. Hasegawa, et al., *Sci. Adv.* **2017**, *3*, e1701126; c) X. Schaapkens, E. O. Bobylev, J. N. H. Reek, et al., *Org. Biomol. Chem.* **2020**, *18*, 4734 – 4738; d) X. Schaapkens, J. H. Holdener, J. Tolboom, et al., *ChemPhysChem* **2021**, https://doi.org/10.1002/cphc.202100229; e) D. Yang, L. K. S. Krbek, L. Yu, et al., *Angew. Chem. Int. Ed.* **2021**, *60*, 4485 – 4490; *Angew. Chem.* **2021**, *133*, 4535 – 4540.

[14] a) D. P. August, G. S. Nichol, P. J. Lusby, *Angew. Chem. Int. Ed.* **2016**, *55*, 15022 – 15026; *Angew. Chem.* **2016**, *128*, 15246 – 15250; b) D. Preston, K. F. White, J. E. M. Lewis, et al., *Chem. Eur. J.* **2017**, *23*, 10559 – 10567; c) L. S. Lisboa, J. A. Findlay, L. J. Wright, et al., *Angew. Chem. Int. Ed.* **2020**, *59*, 11101 – 11107; *Angew. Chem.* **2020**, *132*, 11194 – 11200; d) T. A. Young, V. Marti-Centelles, J. Z. Wang, et al., *J. Am. Chem. Soc.* **2020**, *142*, 1300 – 1310.

[15] a) K. Palanichamy, M. F. Bravo, M. A. Shlain, et al., *Chem. Eur. J.* **2018**, *24*, 13971 – 13982; b) K. Robinson, C. J. Easton, A. F. Dulhunty, et al., *ChemMedChem* **2018**, *13*, 1957 – 1971; c) K. Palanichamy, A. Joshi, T. Mehmetoglu-Gurbuz, et al., *J. Med. Chem.* **2019**, *62*, 4110 – 4119; d) M. F. Bravo, K. Palanichamy, M. A. Shlain, et al., *Chem. Eur. J.* **2020**, *26*, 11782 – 11795.

[16] a) E. S. Feldblum, I. T. Arkin, *Proc. Natl. Acad. Sci. USA* **2014**, *111*, 4085 – 4090; b) I. Rozas, I. Alkorta, J. Elguero, *J. Phys. Chem. A* **1998**, *102*, 9925 – 9932.

Manuscript received: April 13, 2021
Revised manuscript received: April 30, 2021
Accepted manuscript online: May 8, 2021
Version of record online: June 15, 2021

